Mechanics of Materials 135 (2019) 67–76

Contents lists available at ScienceDirect

Mechanics of Materials

journal homepage: www.elsevier.com/locate/mechmat

Smooth waves and shocks of finite amplitude in soft materials

Ron Ziv, Gal Shmuel*

Faculty of Mechanical Engineering, Technion- Israel Institute of Technology, Haifa 32000, Israel

ARTICLE INFO

Keywords:
Smooth wave
Acceleration wave
Shock wave
Soft materials
Rubber
Nonlinear elasticity
Dynamic loading
Gent material
Neo-Hookean material
Finite deformations
Impact

ABSTRACT

Recently developed soft materials exhibit nonlinear wave propagation with potential applications in energy trapping, shock mitigation and wave focusing. We address finitely deformed materials subject to combined transverse and axial impacts, and study the resultant nonlinear waves. We determine the dependency of the induced motion on the impact characteristics, pre-deformation and the employed constitutive models. When using the neo-Hookean constitutive model, we find it cannot capture shear shocks and tensile-induced shocks, in contrast with experimental results on soft materials. Conversely, we find that the Gent model predicts that compressive impact may not be sufficient to induce a quasi-pressure shock—yet it may induce a quasi-shear shock, where tensile impact can trigger quasi-pressure shock—and may simultaneously trigger a quasi-shear shock. These features are in agreement with experimental data. Further, we show that the tensile impact must be greater than a calculated threshold value to induce shock, and demonstrate that this threshold is lowered by application of pre-shear.

1. Introduction

Recent technological advances have promoted the development of soft materials with reconfigurable properties, capable of undergoing reversible finite deformations (Bandyopadhyay et al., 2015; Truby and Lewis, 2016; He et al., 2017; Kim et al., 2017). The nonlinearities associated with these materials give rise to unique transport properties, that can be exploited for tunable dynamic response, energy trapping, shock mitigation and wave focusing (Nadkarni et al., 2014; Shmuel and Band, 2016; Lints et al., 2017; Lustig and Shmuel, 2018; Giammarinaro et al., 2018). These potential applications have led to a revived scientific interest in nonlinear wave propagation of elastic continua (Raney et al., 2016; Xin and Lu, 2016; Deng et al., 2017). The pioneering theoretical work in the field is mainly attributed to Carroll (1967, 1974, 1978), followed by the works of Boulanger and Hayes (1992), Rajagopal (1998) and more recently Destrade and Saccomandi (2005). The focus of these studies is on the existence of harmonic waves with finite amplitude and constant waveforms. Such waves are the exception rather than the rule when nonlinearities are accounted for. Our focus is on finite amplitude smooth waves whose waveform changes in soft materials under impact, which distinguishes what follows from the foregoing studies. Specifically, we study their coalescence to *shocks*—propagating surfaces of discontinuity in the governing fields.

An excellent cover of the research on shocks in solids is given by Davison (2008). One of the central works on shocks in soft materials was by Knowles (2002), who analyzed a one-dimensional bar with cubic stress–strain relation under tensile impact. Using the concept of *thermodynamic driving force*, Knowles theoretically showed that tensile shocks emerge when the impact is sufficiently strong. Niemczura and Ravi-Chandar (2011a,b) have designed and executed corresponding experiments using strips of latex and nitrile rubber. Our objectives are to (*i*) account also for transverse displacements and their coupling with the axial displacements; (*ii*) comprehensively study the effect that combined pre-shear and pre-stretch have on finite amplitude waves induced by simultaneous shear and axial impacts; (*iii*) characterize the dependency of the resultant waves on the constitutive models.

Finite amplitude shocks in similar settings were addressed by several researchers, whose objectives are different that the objectives in this work. Davison (1966) proposed a theory with admissibility conditions for shocks to obtain general formulas and demonstrated his theory using an example problem. Aboudi and Benveniste (1973) developed a finite difference-based scheme to solve the equations governing impact-induced nonlinear waves. Yongchi and Ting (1983) introduced the concept of *stress paths* to determine general solutions, and exemplified their approach using second order isotropic materials. More recently, Scheidler (2000) derived *universal* relations—independent of the specific constitutive relation—between the governing fields and the wave velocities.

In the sequel, we employ the theory of Davison (1966) to obtain and analyze explicit solutions for plane waves of finite amplitude in semi-

* Corresponding author.
E-mail address: meshmuel@technion.ac.il (G. Shmuel).

https://doi.org/10.1016/j.mechmat.2019.05.002
Received 2 January 2019; Received in revised form 5 May 2019
Available online 07 May 2019

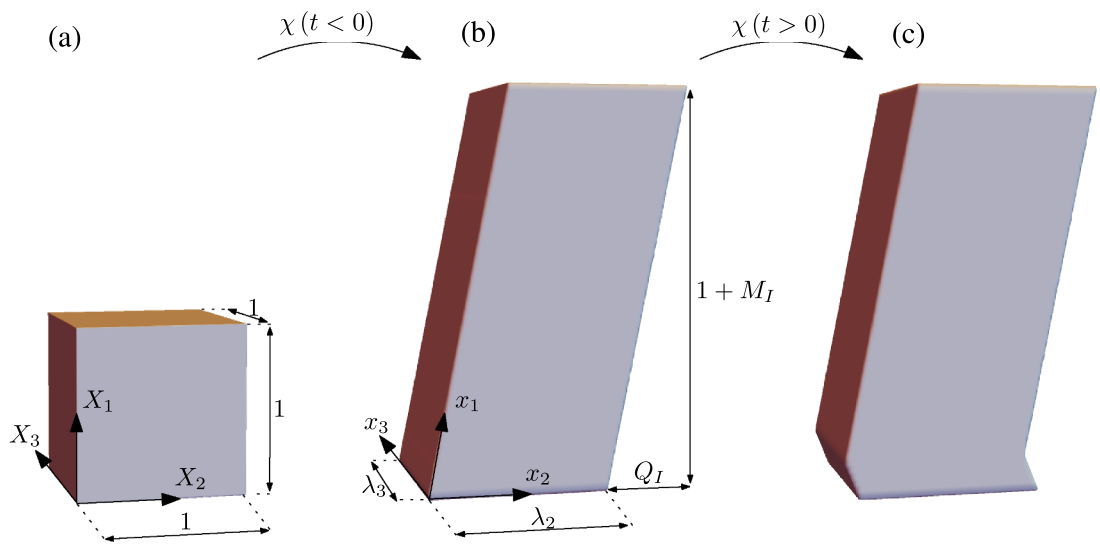

Fig. 1. A unit cube within a semi-infinite body in the (a) reference configuration; (b) pre-deformed configuration under a uniform shear Q_I and axial displacement gradient M_I. (c) Illustrative impact-induced surface of discontinuity at $t > 0$.

infinite soft materials under different pre-deformations and impacts. We employ the two most prominent constitutive models for soft materials—the compressible neo-Hookean and Gent models—to describe the stress–strain relation (Gent, 1996; Puglisi and Saccomandi, 2015). While both models account for finite deformations, the Gent model incorporates an additional nonlinearity, aimed at capturing the stiffening that rubber exhibits due to the limited extensibility of its polymer chains. Interestingly, the Gent model is also useful to describe soft tissues, which stiffen due to the stretching of their collagen fibers (Horgan, 2015). This nonlinearity, in turn, significantly affects the response of the material to impact and formation of shocks, as we show in what follows.

In the limit of small strains, the axial and transverse impact of a semi-infinite medium excites two types of waves, namely, shear and pressure waves. These waves do not interact with each other, and their propagation is independent of the specific loading program and initial state of the material; shocks propagate with the same velocities. By contrast, these waves are generally coupled in finite elasticity, owing to the Poynting effect (Cioroianu and Cornelis, 2013; Horgan and Murphy, 2017); their velocity depends on the constitutive nonlinearity, initial deformation and loading program. In this work, we thoroughly study the effect of these parameters on the propagation of finite amplitude waves.

The findings from the neo-Hookean model are relatively similar to the linear theory, as in the considered settings the model does not capture the coupling between axial and transverse displacements. Specifically, smooth shear waves propagate at a constant velocity as in the linear theory, and cannot evolve to shock. Smooth pressure waves, however, propagate in a velocity that varies as a function of the axial displacement gradient, and coalesce into shock only when the axial impact tends to compress the material, *e.g.*, when a pre-stretched material is released. Accordingly, there are no tensile-induced shocks in neo-Hookean materials. The neo-Hookean predictions are therefore incompatible with experimental data on shear shocks and tensile-induced shocks in soft materials (Catheline et al., 2003; Niemczura and Ravi-Chandar, 2011b).

The predictions of the Gent model are significantly different and more interesting than the neo-Hookean model. Firstly, the model captures the coupling between the transverse and axial motions. We refer to waves at which the only displacement that retained upon linearization is the transverse (resp. axial) displacement as *quasi*-shear (resp. *quasi*-pressure). Their velocities depend both on the initial state and impact program. We characterize this dependency, and determine when they coalesce into shocks. Interestingly, we find that compressive impact may not result in a quasi-pressure shock—yet it may excite a quasi-shear shock, while tensile impact can induce a quasi-pressure shock and a quasi-shear shock at the same time. We show that the tensile impact must be greater than a threshold value to induce shock, and demonstrate that this threshold is lowered when applying pre-shear. Contrary to the neo-Hookean model, the Gent model is able to recover the aforementioned experimental results.

The study is presented in the following order. Section 2 contains the mathematical description of the problem, and its general resolution for smooth and shock wave solutions (Davison, 1966). The generic solution is specialized in Sections 3 and 4, respectively, to the compressible neo-Hookean and Gent models, where we characterize the dependency of the wave velocity on the loading conditions and model parameters, and qualitatively analyze the criterion for shock. Section 5 specializes and quantifies this criterion in terms of the loading parameters, when the material is initially unstrained. Section 6 extends the study of this criterion to finitely strained materials. We conclude this paper with a summary of our results and comments on future work in Section 7.

2. Problem statement and method of solution

The general treatment of the problem using a semi-inverse approach dates back to Davison (1966), which we revisit here for completeness. Consider a semi-infinite soft and compressible material occupying the region $X_1 \geq 0$ in a reference configuration. The material is hyperelastic, such that the 1st Piola–Kirchhoff stress $\mathbf{P}$ is derived from a strain energy function Ψ. Let $\boldsymbol{\chi}$ denote the deformation of material points from a reference coordinate $\mathbf{X}$ to the current coordinate $\mathbf{x}$, where $\mathbf{F} = \nabla_{\mathbf{X}}\boldsymbol{\chi}$ is the deformation gradient, then $\mathbf{P} = \frac{\partial\Psi}{\partial\mathbf{F}}$. We focus on (initially) isotropic materials, for which

$$\mathbf{P} = \alpha_1\mathbf{F} + \alpha_2\mathbf{F}\mathbf{F}^{\mathrm{T}}\mathbf{F} + \alpha_3\mathbf{F}^{-\mathrm{T}} \tag{1}$$

for some response functions α_i that depend on Ψ. At the initial state, the material is sheared and strained along X_1 homogeneously. Subsequently, the body is subjected to a combination of transverse and axial impact at its boundary. Accordingly, the continuous mapping $\boldsymbol{\chi}$ (Fig. 1)

$$x_1 = X_1 + u_1(X_1, t),\ \ x_2 = X_2 + u_2(X_1, t),\ \ x_3 = X_3, \tag{2}$$

is subjected to the initial and boundary conditions

$$\frac{\partial u_1}{\partial X_1}(0,\,t) = \{M_I t \le 0 M_B t > 0 = :M(0,\,t),\ \ \frac{\partial u_2}{\partial X_1}(0,\,t) = \{Q_I t \le 0 Q_B t > 0$$
$$= :Q(0,\,t),\ \frac{\partial u_1}{\partial t}(0,\,t) = \{0t \le 0 R_B t > 0 = :R(0,\,t),$$
$$\frac{\partial u_2}{\partial t}(0,\,t) = \{0t \le 0 S_B t > 0 = :S(0,\,t); \tag{3}$$

the fields M, Q, R and S are the axial displacement gradient, transverse displacement gradient, axial velocity and transverse velocity, respectively, where we recall that at $t = 0$ the fields are homogeneous. Thus, Eq. (3) describes a semi-infinite body that is initially strained with a uniform shear Q_I and axial displacement gradient M_I, and subjected to a combination of transverse and axial impacts, denoted by Q_B and M_B, respectively; further, the transverse and axial velocities at the boundary are denoted by S_B and R_B, respectively. The problem at hand is to determine the resultant motion $u_i(X_1,\,t)$ for $t > 0$.

2.1. Smooth and acceleration wave solutions

Assuming $\boldsymbol{\chi}$ is continuously differentiable twice almost everywhere, the differential equations governing the problem (except at singular surfaces) are

$$\nabla_{\mathbf{X}}\cdot\mathbf{P} = \rho_L \chi_{,tt}, \tag{4}$$

where $\rho_L = J\rho$, $J = \det\mathbf{F}$ and ρ is the current mass density. Eq. (4) takes the form

$$P_{11,1} = \rho_L \frac{\partial^2 x_1}{\partial t^2},\ \ P_{21,1} = \rho_L \frac{\partial^2 x_2}{\partial t^2}, \tag{5}$$

for the motion considered in Eq. (2), and the constitutive form (1). We use the variables R, M, Q and S defined in Eq. (3) to reduce the order of Eq. (5) and obtain

$$P_{11,1} = \rho_L R_{,t},\ \ P_{21,1} = \rho_L S_{,t},\ M_{,t} = R_{,1},\ \ Q_{,t} = S_{,1}. \tag{6}$$

By application of the chain rule, we rewrite Eq. $(6)_{1,2}$ as

$$\alpha M_{,1} + \beta Q_{,1} = R_{,t},\ \gamma M_{,1} + \delta Q_{,1} = S_{,t}, \tag{7}$$

where

$$\alpha = \frac{1}{\rho_L}\frac{\partial P_{11}}{\partial M},\ \ \beta = \frac{1}{\rho_L}\frac{\partial P_{11}}{\partial Q},\ \ \gamma = \frac{1}{\rho_L}\frac{\partial P_{21}}{\partial M},\ \ \delta = \frac{1}{\rho_L}\frac{\partial P_{21}}{\partial Q}. \tag{8}$$

We firstly seek smooth wave solutions that depend on a single independent variable. We set this variable to be $c = X_1/t$, and obtain

$$\alpha M_{,c} + \beta Q_{,c} + cR_{,c} = 0,\ \ \gamma M_{,c} + \delta Q_{,c} + cS_{,c} = 0,\ R_{,c} + cM_{,c} = 0,$$
$$S_{,c} + cQ_{,c} = 0, \tag{9}$$

from Eqs. $(6)_{3,4}$ and (7). Substitution of Eqs. $(9)_3$ and $(9)_4$ into Eqs. $(9)_1$ and $(9)_2$, respectively, provides

$$(\alpha - c^2)M_{,c} + \beta Q_{,c} = 0,\ \gamma M_{,c} + (\delta - c^2)Q_{,c} = 0. \tag{10}$$

These equations have a non-trivial solution only if

$$c^4 - (\alpha - \delta)^2 c^2 + \alpha\delta - \beta\gamma = 0. \tag{11}$$

Solving for c gives the characteristic wave velocities[1]

$$c^2 = \frac{1}{2}[\alpha + \delta \pm \sqrt{(\alpha - \delta)^2 + 4\beta\gamma}\,] = :c_\pm^2. \tag{12}$$

In the limit of linear elasticity, the velocities c_+ and c_- reduce to the velocities of pressure and shear waves, respectively. In this limit $c_+ = \sqrt{\alpha}$, $c_- = \sqrt{\delta}$, $\beta\gamma = 0$, and accordingly there is no coupling through the equations of motion between the corresponding waves.

We refer to the slow and fast smooth waves associated with c_- and c_+ as *quasi*-shear and *quasi*-pressure waves, respectively. We assume that these waves spatially expand in the course of propagation, as illustrated in Fig. 2(a) by the gray regions. We further assume that fields in the white cones separating these waves and the rays $t = 0$ and $X_1 = 0$ are uniform. The cone that is bounded by $t = 0$ (resp. $X_1 = 0$) is denoted by $\mathcal{B}$ (resp. $\mathcal{I}$). The middle cone is denoted by $\mathcal{U}$. The fields in these regions are denoted with the subscripts B, I and U. To determine the velocity field in between the front ($X_1 = V_{SU}t$) and back ($X_1 = V_{BS}t$) characteristics of the quasi-shear wave, we substitute c_- back into Eq. (10) and obtain

$$\frac{\mathrm{d}M}{\mathrm{d}Q} = -\frac{\beta}{\alpha - c_-^2}. \tag{13}$$

These characteristics define surfaces of discontinuity for the second derivatives of u_i, and are termed *acceleration* waves. The first derivatives are continuous, and thus Eq. (13) is subjected to a *compatibility* condition in the form of the continuity of M, such that $M(Q = Q_B) = M_B$, where we recall that c_- is a function of M and Q. Similarly, to determine the velocity field in between the front ($X_1 = V_{PI}t$) and back ($X_1 = V_{UP}t$) characteristics of the quasi-pressure wave we substitute c_+ back into Eq. (10) and obtain

$$\frac{\mathrm{d}Q}{\mathrm{d}M} = -\frac{\alpha - c_+^2}{\beta}, \tag{14}$$

subjected to the compatibility condition $Q(M = M_I) = Q_I$ for the acceleration waves. Let Q_+ (resp. Q_-) denote the value of Q at the back (resp. front) of the quasi-pressure (resp. shear) wave; the continuity condition between the shear and pressure waves is then reads $Q_+ = Q_- = :Q_U$.

2.2. Shock wave solutions

Smooth waves bounded by acceleration waves evolve only when the calculated velocity at the back of the wave is smaller than the velocity at the front of the wave, and changes monotonically in between. This requirement can be written as

$$V_{BS} < c_-(Q) < V_{SU},\ \ \frac{\mathrm{d}c_-}{\mathrm{d}Q} \ne 0 \quad \forall\, Q \in (Q_B,\, Q_U),\ V_{UP} < c_+(M) < V_{PI},$$
$$\frac{\mathrm{d}c_+}{\mathrm{d}M} \ne 0 \quad \forall\, M \in (M_U,\, M_I). \tag{15}$$

Shocks evolve when conditions (15) fail to hold, and define a surface of discontinuity for all the governing fields except the displacements. We restrict attention to the cases when either $V_{BS} < c_-(Q) < V_{SU}$ and/or $V_{BS} < c_-(Q) < V_{SU}$ are violated. The integral form of Eq. (4) is then used to derive the jump conditions

$$\rho_L[\![R]\!]V + [\![P_{11}]\!] = 0,\ \ [\![M]\!]V + [\![R]\!] = 0,\ \rho_L[\![S]\!]V + [\![P_{21}]\!] = 0,$$
$$[\![Q]\!]V + [\![S]\!] = 0; \tag{16}$$

here, V is the shock velocity and $[\![\circ]\!]$ is the jump in $(\circ)$ between the regions ahead and behind the shock. Specialization of Eq. (16) to the loading (3) delivers the following conditions for the quasi-shear shock and quasi-pressure shock waves

$$[\![P_{11}]\!]_{UB}[\![Q]\!]_{UB} - [\![P_{21}]\!]_{UB}[\![M]\!]_{UB} = 0,\ [\![P_{11}]\!]_{IU}[\![Q]\!]_{IU} - [\![P_{21}]\!]_{IU}[\![M]\!]_{IU} = 0, \tag{17}$$

respectively, where paired subscripts of $[\![\circ]\!]$ denote that the jump is between the corresponding regions; each of these equations provides a connection between Q_U and M_U. The shock velocities resulting from Eq. (16) are

$$V_S = \sqrt{\frac{[\![P_{21}]\!]_{UB}}{\rho_L[\![Q]\!]_{UB}}},\ \ V_P = \sqrt{\frac{[\![P_{11}]\!]_{IU}}{\rho_L[\![M]\!]_{IU}}}, \tag{18}$$

where V_S and V_P correspond to the quasi-shear and quasi-pressure shock velocities, respectively. Depending on the loading program and

[1] These velocities are *Lagrangian*, measured relative to the reference coordinate X_1. The *Eulerian* velocities, measured with respect to the moving coordinate x_1, are $(1 + M)c_\pm$ (Davison, 2008).

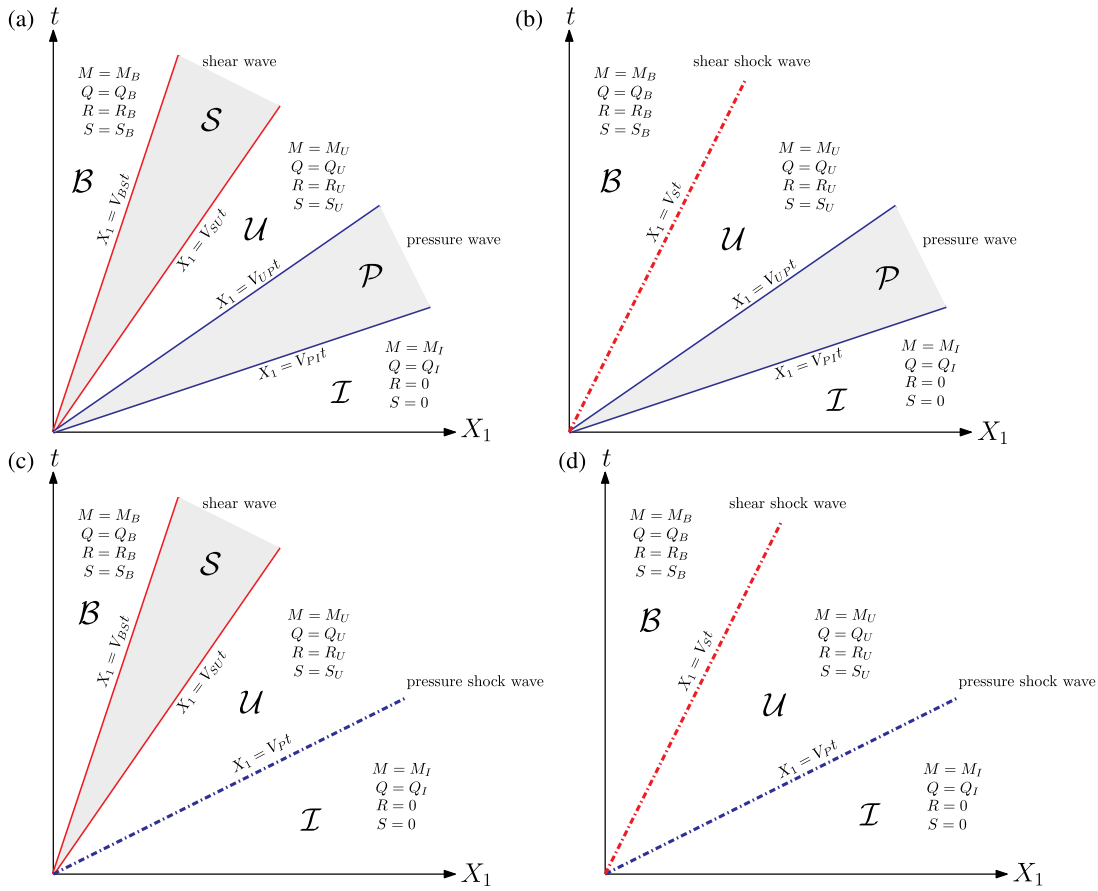

Fig. 2. Characteristic curves as solutions to boundary and initial conditions. For monotonic c, the solution to the quasi-shear and quasi-pressure waves is one of the following combinations: (a) smooth-smooth, (b) shock-smooth, (c) smooth-shock, (d) shock-shock, depending on the boundary and initial conditions. Dot-dashed and continuous curves correspond to shock and acceleration waves solutions, respectively. Smooth waves are denoted in gray.

the specific constitutive behavior, four combinations of shear and pressure waves can develop, *i.e.*, smooth-smooth (Fig. 2a), shock-smooth (Fig. 2b), smooth-shock (Fig. 2c), and shock-shock (Fig. 2d). In general, the theory does not identify *a priori* which combination takes place. The course taken is to use a semi-inverse method of solution, *i.e.*, firstly assume smooth-smooth solutions, and examine the compatibility of the corresponding set of equations. If the compatibility fails to hold, we assume that shock-smooth waves propagate, and examine the compatibility of the corresponding equations. This process is continued until we find a compatible set and identify the combination that takes place. The foregoing combinations cover all the possibilities when c is monotonic.

3. Analysis of compressible neo-Hookean materials

The study of smooth waves and shocks of finite amplitude in neo-Hookean and Gent materials is carried out next, using the theory in Section 2. We begin with the neo-Hookean model

$$\Psi = \frac{\mu}{2}(I_1 - 3) - \mu \ln J + \left(\frac{\kappa}{2} - \frac{\mu}{3}\right)(J-1)^2, \tag{19}$$

where $I_1 = \mathrm{tr}\mathbf{F}^{\mathrm{T}}\mathbf{F}$, and κ and μ correspond to the bulk and shear moduli, respectively, in the limit of small strains. For this model, the velocities obtained from Eq. (12) are

$$c_- = \sqrt{\delta} = \sqrt{\frac{\mu}{\rho_L}}, \quad c_+ = \sqrt{\alpha} = \sqrt{\frac{\kappa}{\rho_L} + \frac{\mu(M^2 + 2M + 4)}{3\rho_L(M+1)^2}}. \tag{20}$$

Notably, since $\beta\gamma = 0$ the velocities and corresponding waves are not coupled. Stated differently, the axial displacement gradient M and shear field Q evolve independently in the material.

The neo-Hookean model predicts that (pure) smooth shear waves propagate with a constant velocity, and hence cannot evolve to shock. Therefore, the model is incompatible with experimental demonstrations of shear shocks in soft solids (Catheline et al., 2003; Jacob et al., 2007).

The neo-Hookean model predicts that (pure) pressure waves propagate as smooth waves with the velocity c_+ only if $M_B > M_I$, since c_+ is a monotonically decreasing function of M. Mechanically speaking, the mathematical condition implies that only compressive impact leads to shock. Accordingly, the neo-Hookean model is incapable of recovering experimental data of tensile-induced shocks in soft materials (Kolsky, 1969; Niemczura and Ravi-Chandar, 2011b). The dependency of c_+ on M is exemplified in Fig. 3(a), which shows c_+ as a function of M (dashed-blue curve), for the representative parameters

$$\kappa = 1\mathrm{MPa}, \ \mu = 200\mathrm{kPa}, \ \rho_L = 1000\mathrm{kg/m^3}; \tag{21}$$

for comparison, the shear wave velocity is also displayed (orange line). To complete the solution, we need to determine M_U and Q_U; owing to the decoupling of the velocities, we have that $M_U = M_B$ and $Q_U = Q_I$. If $M_B < M_I$, then the pressure wave will coalesce into shock with the velocity $(18)_2$.

By way of example, we examine a material at the initial compression state $M_I = -0.4$ and consider two different impacts at the boundary, namely $M_{B_1} = -0.6$ and $M_{B_2} = 0.1$. These impacts are indicated in panel 3(a) by the triangle (M_{B_1}) and square (M_{B_2}) marks. The former propagates as shock with the velocity $V_P = 43.58$m/s, since $M_{B_1} < M_I$. The latter propagates as a smooth wave with the velocity range $35.01\mathrm{m/s} < c_+(M) < 40.27\mathrm{m/s}$. The corresponding distributions along X_1 of M for the two boundary conditions at $t = 1$ms (solid curves)

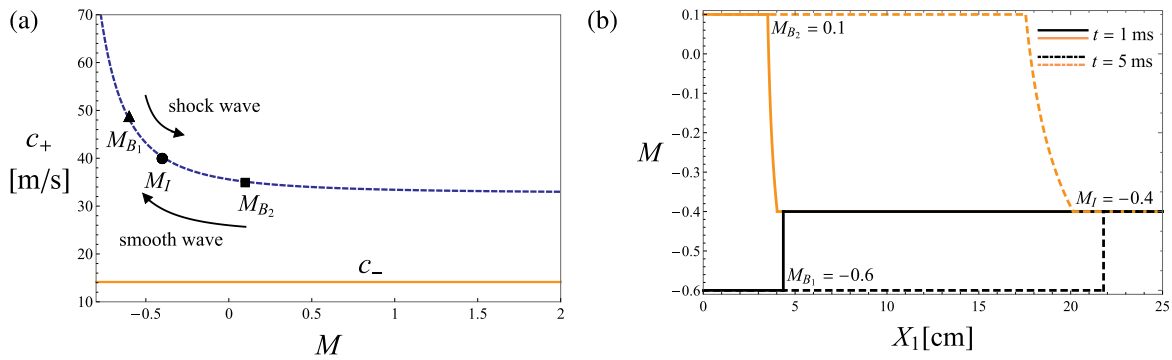

Fig. 3. (a) Pressure (dashed-blue curve) and shear (orange line) wave velocities as functions of M, for a neo-Hookean material with the material parameters (21). The triangle (M_{B_1}) and square (M_{B_2}) marks correspond to boundary conditions that result in smooth and shock waves, respectively, when the initial condition is $M_I = -0.4$ (circle mark). (b) Corresponding distributions along X_1 of the axial displacement gradient M for M_{B_1} (black) and M_{B_2} (orange) at $t = 1$ms (solid curves) and $t = 5$ms (dashed curves). (For interpretation of the references to color in this figure legend, the reader is referred to the web version of this article.)

and $t = 5$ms (dashed curves) are shown in Fig. 3(b). We observe that indeed M_{B_1}(black) is associated with the propagation of strain discontinuity. Conversely, applying M_{B_2} (orange) yields smooth spreading of strain bounded between acceleration waves, identified by discontinuities in the derivative of M.

4. Analysis of compressible Gent materials

The second model we employ is the compressible Gent model (Gent, 1996). This model successfully captures the stiffening of elastomers at high strains due to the finite extensibility of their polymer chains. At the same time, it is a simple three-parameter model that enables in certain cases the derivation of analytical solutions, which makes it a popular model in soft elasticity (Horgan, 2015; Puglisi and Saccomandi, 2015). The corresponding Gent strain energy density is (Lopez-Pamies and Castañeda, 2007)

$$\Psi = -\frac{\mu}{2}J_m \ln\left(1 - \frac{I_1 - 3}{J_m}\right) - \mu \ln J + \left(\frac{\kappa}{2} - \frac{\mu}{3} - \frac{\mu}{J_m}\right)(J-1)^2, \tag{22}$$

where J_m models the elastomeric strain stiffening; in the limit $J_m \to \infty$, the neo-Hookean model is recovered. Application of Eq. (12) to the Gent model (22) provides the velocities

$$c_\pm^2 = \frac{a_3}{2\rho_L} + \frac{\mu}{2\rho_L a_1^2} + \frac{(a_1^2 + Q^2 + J_m)\mu J_m}{2\rho_L a_2^2} \pm \frac{\sqrt{48 a_1^6 \mu^2 Q^2 J_m^2 + (a_1^2 a_2^2 a_3 + 2a_1^4 \mu J_m - 2a_1^2 Q^2 \mu J_m + a_2^2 \mu)^2}}{2\sqrt{3}\rho_L a_2^2 a_1^2}, \tag{23}$$

where $a_1 = M + 1$, $a_2 = M^2 + 2M + Q^2 - J_m$, and $a_3 = \kappa - \frac{2\mu}{3} - \frac{2\mu}{J_m}$. Notably, both c_+ and c_- depend nonlinearly on Q and M. These velocities, in turn, yield nonlinear differential Eqs. (13) and (14) for $Q(M)$ and $M(Q)$, which cannot be solved analytically. To investigate the dependency of the velocities on the parameters of the problem, we use numerical solutions obtained by the Runge–Kutta solver of the software Wolfram Mathematica 11.3 (2018).

We begin with the study of c_- in Fig. 4. In Panel 4(a) we evaluate c_- as a function of Q for the parameters in Eq. (21) and $J_m = 10$, at different impacts. Specifically, we evaluate c_- for the boundary conditions $Q_B = 0$, $M_B = 0$ (solid black), $Q_B = 1$, $M_B = 0$ (dashed blue) and $Q_B = 2$, $M_B = -0.6$ (dot-dashed brown). We observe that the boundary conditions have little effect on the curve of c_-, which is a monotonically increasing function of Q. As we will demonstrate in panels 4(b)–(d), this monotonicity is independent of the specific material parameters. Therefore, shear impact *loading* results in a shock, while shear impact *unloading* results in a smooth wave. We recall that this phenomenon cannot be captured by the neo-Hookean model, where shear shock cannot evolve. Panel 4(b) shows $c_-(Q)$ for $Q_B = 0$, $M_B = 0$, and different values of the locking parameter J_m. Specifically, the solid black, dashed cyan, dot-dashed brown, and dashed blue curves correspond to $J_m = 10$, 15, 30 and $J_m \to \infty$, respectively. We observe that the velocity decreases as J_m increases, while its monotonicity in Q is maintained. In the limit $J_m \to \infty$ the velocity is independent of Q, thereby recovering the neo-Hookean response, as it should.

Panel 4(c) shows $c_-(Q)$ for $Q_B = 0$, $M_B = 0$, and different values of the shear modulus μ. Specifically, the solid black, dashed cyan and dot-dashed brown curves correspond to $\mu = 0.2$MPa, 0.5MPa and 1MPa, respectively. The velocity is greater for higher values of μ, as expected. Here again, the monotonicity in Q is kept.

Panel 4(d) shows $c_-(Q)$ for $Q_B = 0$, $M_B = 0$, and different values of the bulk modulus κ. Specifically, the solid black, dashed cyan and dot-dashed brown curves correspond to $\kappa = 0.5$MPa, 1MPa and 5MPa, respectively. At small amounts of shear ($Q \le 1.5$), the velocity is independent of κ. When the material is severely sheared ($Q > 1.5$), the coupling between the modes becomes substantial, and the quasi-shear velocity is higher in materials with greater bulk modulus. Again, independently of κ, the velocity is a monotonically increasing function of Q.

We analyze next the quasi-pressure wave velocity c_+ in Fig. 5. Panel 5(a) shows c_+ as function of M for the initial conditions $Q_I = 0$, $M_I = 0$ (solid black), $Q_I = 1$, $M_I = 0$ (dashed cyan), and $Q_I = 2$, $M_I = -0.6$ (dot-dashed brown). Contrary to the monotonicity of c_-, we observe that beyond a critical deformation, denoted M_{cr}, the curve changes its trend from downward to upward. The value of M_{cr} decreases for greater values of Q_I. Since the condition for smooth waves depends on the sign of $\frac{dc_+}{dM}$ and the location of M_U, M_I and M_{cr}, we can deduce if shocks emerge from this diagram, as we will demonstrate later.

Panel 5(b) shows $c_+(M)$ for $Q_I = 0$, $M_I = 0$, and different values of the locking parameter J_m. The legend is identical to the legend in panel 4(b). We observe that the slope beyond M_{cr} decreases as J_m increases, until it vanishes in the limit $J_m \to \infty$, thereby recovering the neo-Hookean response, as it should.

Panel 5(c) shows $c_+(M)$ for $Q_I = 0$, $M_I = 0$, and different values of the shear modulus μ. The legend is identical to the legend in panel 4(c). The velocity is higher for greater values of μ, while the value of M_{cr} remains unchanged.

Panel 5(d) shows $c_+(M)$ for $Q_I = 0$, $M_I = 0$, and different values of the bulk modulus κ. The legend is identical to the legend in panel 4(d). As expected, the velocity is higher when κ is greater, where the difference decreases as the strain increases. We observe that the value of M_{cr} is independent of κ.

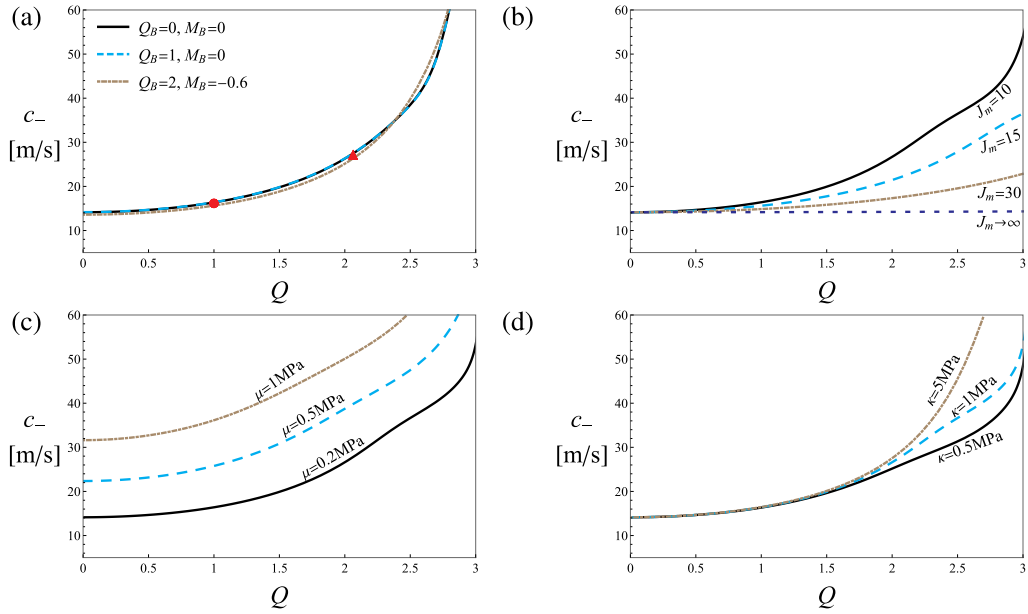

Fig. 4. The quasi-shear wave velocity c_- as function of Q, for the Gent material at the boundary conditions $Q_B = 0,\ M_B = 0$, material parameters (21) and $J_m = 10$. Each panel shows c_- for different values of the (a) boundary conditions: $Q_B = 0,\ M_B = 0$ (solid black), $Q_B = 1,\ M_B = 0$ (dashed cyan) and $Q_B = 2,\ M_B = -0.6$ (dot-dashed brown); (b) locking parameter: $J_m = 10$ (solid black), 25 (dashed cyan), 30 (dot-dashed brown) and ∞ (blue dashed); (c) shear modulus: $\mu = 0.2$MPa (solid black), 0.5MPa (dashed cyan) and 1MPa (dot-dashed brown); (d) bulk modulus: $\kappa = 0.5$MPa (solid black), 1MPa (dashed cyan) and 5MPa (dot-dashed brown). (For interpretation of the references to color in this figure legend, the reader is referred to the web version of this article.)

5. Combined shear and axial impact of unstrained materials

We provide next a more comprehensive analysis of the effect of the boundary conditions Q_B and M_B on waves in unstrained materials ($M_I = 0,\ Q_I = 0$), starting with quasi-shear waves. We recall that shear waves in neo-Hookean materials always propagate as smooth waves, since c_- is constant. To analyze quasi-shear waves in Gent materials, we utilize Fig. 4(a), to deduce that these waves will always propagate as shocks, since $\frac{dc_-}{dQ} > 0$ for any $Q_B > 0 = Q_I$.

We proceed with the analysis of the effect on quasi-pressure waves, which requires the calculation of M_U. As stated in Section 3, the value

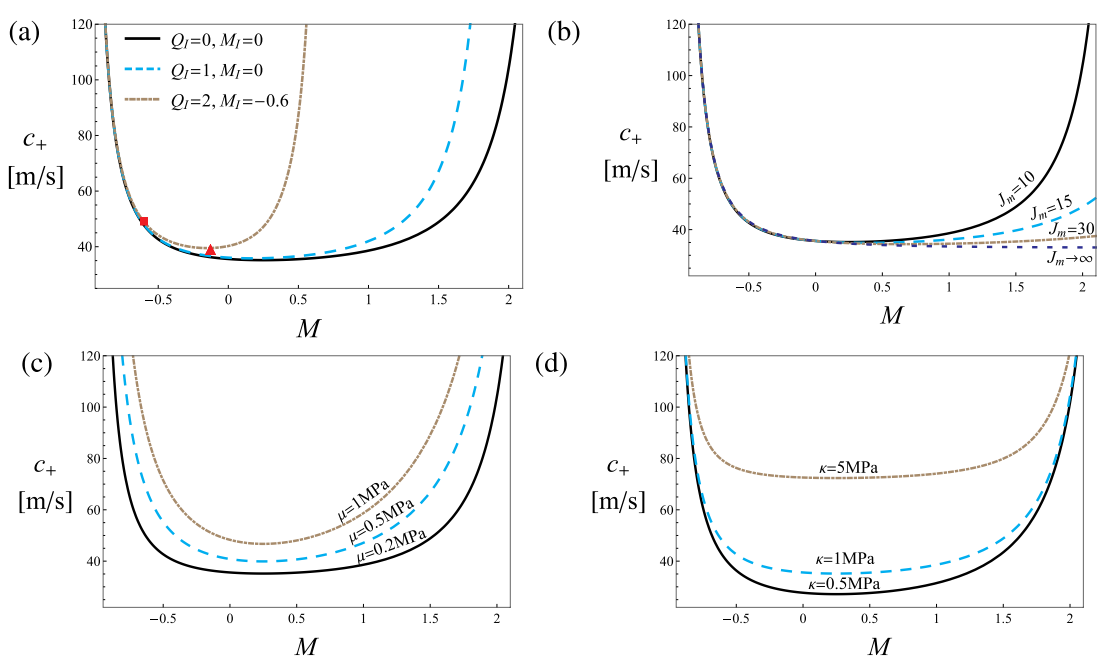

Fig. 5. The pressure wave velocity c_+ as function of M, for the Gent material at the boundary conditions $Q_B = 0,\ M_B = 0$, material parameters (21) and $J_m = 10$. Each panel shows c_+ for different values of the (a) boundary conditions: $Q_B = 0,\ M_B = 0$ (solid black), $Q_B = 1,\ M_B = 0$ (dashed cyan) and $Q_B = 2,\ M_B = -0.6$ (dot-dashed brown); (b) locking parameter: $J_m = 10$ (solid black), 25 (dashed cyan), 30 (dot-dashed brown) and ∞ (dashed blue); (c) shear modulus: $\mu = 0.2$MPa (solid black), 0.5MPa (dashed cyan) and 1MPa (dot-dashed brown); (d) bulk modulus: $\kappa = 0.5$MPa (solid black), 1MPa (dashed cyan) and 5MPa (dot-dashed brown). (For interpretation of the references to color in this figure legend, the reader is referred to the web version of this article.)

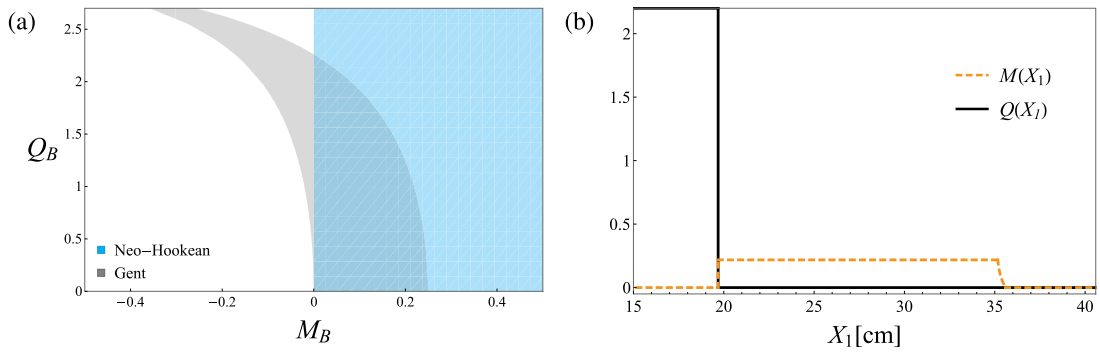

Fig. 6. (a) Impacts that yield smooth pressure waves in unstrained materials as regions in the (M_B, Q_B)-plane. Cyan and Gray denote neo-Hookean and Gent materials, respectively. The material parameters are given in Eq. (21), where for the Gent material we also set $J_m = 10$. (b) Shock-smooth wave solutions for an unstrained Gent material, for the boundary conditions $M_B = 0$, $Q_B = 2.2$. (b) the strain fields M (dashed orange) and Q (solid black) from the shock-smooth wave due to the impact $(M_B, Q_B) = (0, 2.2)$ at $t = 10$ ms.

for neo-Hookean materials is simply $M_U = M_B$, since the waves are not coupled. Then, independently of Q_B and for any $M_B < 0$, pressure shocks emerge, since $\frac{dc_+}{dM} < 0$ from $M_B < 0$ to $M_I = 0$ (Fig. 3a). Hence, in the (Q_B, M_B)-plane we identify loadings that result in smooth quasi-pressure waves with the half-space $M_B > 0$, as illustrated in Fig. 6(a) by the cyan color. Thus, only compressive impacts create shocks. Again we note that this is incompatible with experiments showing tensile-induced shocks.

The value of M_U in Gent materials depends on M_B *and* Q_B, due to the coupling between the fields, and requires the use of Eq. $(17)_1$. Note that $Q_U = 0$ in Eq. $(17)_1$, since we assume that the shear impact is slower than V_{SU}. Smooth quasi-pressure waves propagate when $0 < M_U < M_{cr}$, since in this interval $\frac{dc_+}{dM} < 0$, as illustrated in Fig. 5(a). Conversely, quasi-pressure shocks propagate when $M_{cr} < M_U$, since in this interval c_+ losses its monotonicity. The combinations of Q_B and M_B that yield $0 < M_U < M_{cr}$ and smooth quasi-pressure waves are illustrated in Fig. 6(a) on the (M_B, Q_B)-plane by the gray color. Interestingly, in the absence of shear impact ($Q_B = 0$), there exists a threshold value of tensile impact ($M_B = 0.25$) above which shocks emerge. In other words, the Gent model predicts that sufficiently strong tensile impacts induce shocks. Notably, Knowles (2002) arrived to the same conclusion when analyzing the tensile impact of soft rods with cubic stress–strain equation, using the concept of thermodynamic driving force. We observe that the threshold value of the tensile impact for shock is lowered by applying simultaneously shear impact. Furthermore, the application of shear impact creates a threshold value for compressive impacts, below which shocks cannot evolve. We conclude this part by evaluating in panel 6(b) the strain fields M (dashed orange) and Q (solid black) from the shock-smooth wave at the boundary conditions $(M_B, Q_B) = (0, 2.2)$ at $t = 10$ ms[2] We observe that the quasi-shear shock excites also axial strains ($19.5\,\text{cm} < X_1 < 35.5\,\text{cm}$), and the quasi-pressure smooth wave is not accompanied with shear strains ($35\,\text{cm} < X_1 < 35.5\,\text{cm}$).

6. Combined shear and axial impact of finitely strained materials

We complete our study by analyzing more extensively the general case of pre-strained materials subjected to combined impact. We recall that for neo-Hookean materials, the field M_U is independent of M_I and Q_I, hence we focus on Gent materials. The complexity of the corresponding analysis stems from the fact that we do not know *a priori* which kind of combination of waves develops, since M_U and Q_U are functions of all the prescribed quantities $\{M_I, Q_I, M_B, Q_B\}$, and M_{cr} depends on M_I and Q_I. As mentioned in Section 2, we proceed by assuming that the combination is smooth-smooth (Fig. 2a). We solve Eqs. (13) and (14) to determine M_U and Q_U and examine if our assumption holds via Eq. (15); otherwise, we assume the combination is shock-smooth (Fig. 2b), and solve Eqs. (14) and $(17)_1$ to determine M_U and Q_U, and examine if our solution satisfies Eq. (15) and so forth, until we find a compatible set. We illustrate in Fig. 7 the resultant wave classification as functions of M_B and Q_B for Gent materials with the properties (21) and $J_m = 10$. Specifically, panels 7(a)–(d) correspond to $(M_I, Q_I) = (0, 1.5)$, $(0, 1.71)$, $(0, 2)$, $(-0.2, 0.5)$, $(0, 0.5)$, and $(0.1, 0.5)$, respectively. The blue, green, orange and red regions correspond to smooth-smooth, shock-smooth, smooth-shock and shock-shock, respectively. The white regions correspond to impacts for shocks evolve due to loss of monotonicity of c_+, and are outside our scope.

We observe that by moving vertically up (resp. down), *i.e.*, imparting shear loading (resp. unloading) impact, we always enter a quasi-shear shock (resp. smooth) region[3] During shear impact we may or may not enter a quasi-pressure shock region, depending on the initial strain. For instance, in panel 7(a), shear loading impact results in smooth quasi-pressure waves, while in panel 7(c) it results in quasi-pressure shocks. These panels demonstrate that the results are reversed upon impact unloading.

The effect of axial impacts is more complex. Specifically, compressive impact and tensile impact may or may not trigger quasi-pressure shock, depending on the initial state. For example, panel 7(a) shows that only compressive impact induces quasi-pressure shock when the pre-strain is $Q_I = 1.5$; when the initial shear is increased to 2 (panel 7 c), the trend is reversed, *i.e.*, only tensile impact results in quasi-pressure shock. Panel 7(b) shows a unique state of initial shear ($Q_I = 1.7$), at which any axial impact will create quasi-pressure shock. As pointed out in Section 4, the value of M_{cr} decreases as Q_I increases, and for $Q_I = 1.7$ its value is 0. This implies that in a material that was strained accordingly, any axial impact will propagate faster than $c_+(M_I = 0)$, hence coalesce into shock.

By comparing panels 7(d)–(f) where Q_I is fixed and M_I is increased, we observe that M_I has little effect on the value of M_{cr} and the threshold value of impact for tensile shock. The curve that separates regions of quasi-pressure smooth waves from corresponding shocks passes through M_I, and when $M_I > 0$ (resp. $M_I < 0$) the region of impact that creates smooth quasi-pressure waves is narrower (resp. wider).

[2] The procedure of obtaining M_U for $(M_I, Q_I, M_B, Q_B) = (0, 0, 0.2. 2)$ is illustrated in Appendix A.

[3] The admissibility conditions for quasi-shear waves hold also in the white regions next to the blue regions. The admissibility conditions for the quasi-shear waves is violated in the white regions next to the green regions.

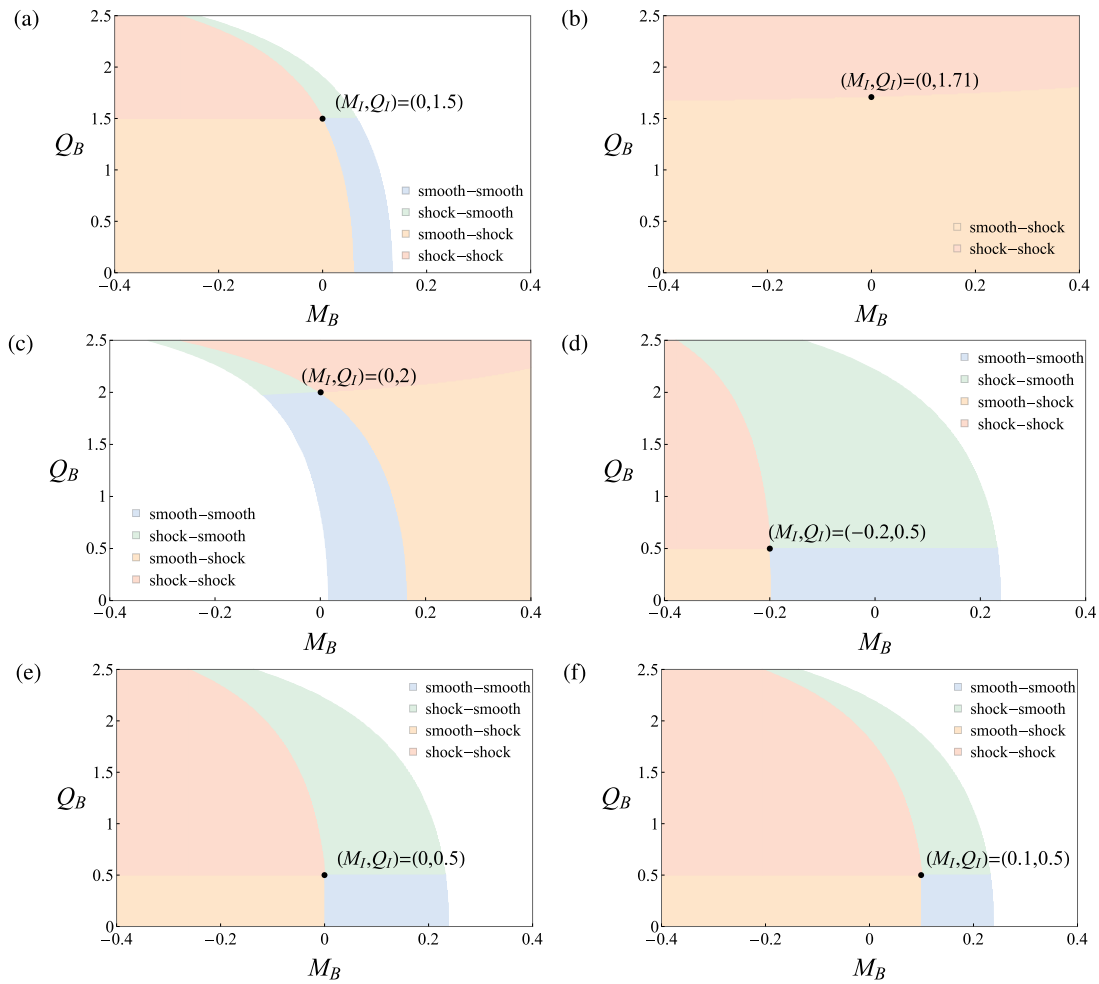

Fig. 7. Regions in the (M_B, Q_B)-plane that induce smooth-smooth (blue), shock-smooth (green), smooth-shock (orange), and shock-shock (red) waves in Gent materials with the properties (21) and $J_m = 10$. Panels (a)-(f) correspond to $(M_I, Q_I) = (0, 1.5)$, $(0, 1.71)$, $(0, 2)$, $(-0.2, 0.5)$, $(0, 0.5)$, and $(0.1, 0.5)$, respectively. (For interpretation of the references to color in this figure legend, the reader is referred to the web version of this article.)

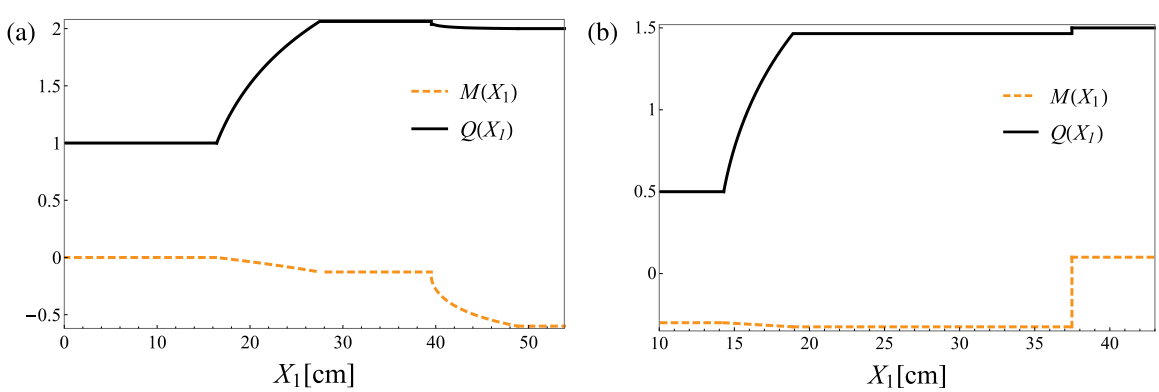

Fig. 8. Wave solutions for a Gent material with the parameters $\kappa = 1$ MPa, $\mu = 200$ kPa, $\rho_L = 1000$ kg/m^3, $J_m = 10$. Each panel shows M (solid-black) and Q (dashed-orange) as function of X_1, at $t = 10$ms, for the conditions (a) $M_I = -0.6$, $Q_I = 2$, $M_B = 0$, $Q_B = 1$; (b) $M_I = 0.1$, $Q_I = 1.5$, $M_B = -0.3$, $Q_B = 0.5$.

We conclude our study by evaluating in Fig. 8 the strain fields M (dashed orange) and Q (solid black) from the smooth-smooth (panel 8a) and smooth-shock (panel 8b) waves at the conditions $(M_I, Q_I, M_B, Q_B) = (-0.6, 2, 0, 1)$[4] and $(0.1, 1.5, -0.3, 0.5)$, respectively. Evidently, quasi-shear waves excite also axial strains, *e.g.*, the interval $16\,\text{cm} < X_1 < 28\,\text{cm}$ in panel 8(a), and quasi-pressure shocks excite also shear strains, *e.g.*, $X_1 = 35\,\text{cm}$ in panel 8(b).

[4] The procedure of obtaining M_U for $(M_I, Q_I, M_B, Q_B) = (-0.6, 2, 0, 1)$ is illustrated in Appendix A.

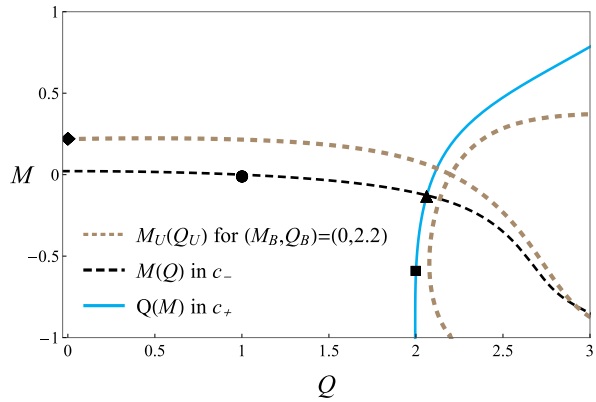

Fig. 9. Pairs of (M_U, Q_U) that solve Eq. (17)$_1$ for the boundary values $(M_B, Q_B) = (0, 2.2)$ are denoted in brown. The value of $M_U(Q_U = Q_I = 0)$ is denoted by the diamond mark. Solutions of Eqs. (13) and (14) are given by the dashed-black and solid-cyan, for $(M_I, Q_I, M_B, Q_B) = (-0.6, 2, 0, 1)$. The circle, triangle and square correspond to Q_B, Q_U and Q_I, respectively.

7. Summary

The general aim was to study smooth and shock waves of finite amplitude in soft materials described by the two most prominent constitutive models, namely, the neo-Hookean and Gent models (Gent, 1996). Our study was carried out for the plane motion of a finitely strained semi-infinite material, in response to combined transverse and axial impacts. Our specific objective was to characterize the effect of the constitutive modeling, pre-deformation and impact program have on resultant waves.

The analysis of the neo-Hookean model provided the following observations. We found that the resultant axial and transverse motions in neo-Hookean materials are uncoupled. Independently of the specific boundary conditions, smooth shear waves propagate at a constant velocity, and thus cannot coalesce into shock. The velocity of smooth pressure waves is a monotonically decreasing function of the axial impact, hence coalesce into shock when the impact compresses the material, as expected. These observations infer that the neo-Hookean model is not adequate to describe experimental results on shear shocks and tensile-induced shocks in soft materials (Catheline et al., 2003; Niemczura and Ravi-Chandar, 2011b).

The analysis of the Gent model is more complex, exhibiting richer results. We found that the model predicts that the resultant axial and transverse motions are coupled such that an axial (resp. transverse) impact will also create transverse (resp. axial) displacements. Contrary to the neo-Hookean model, the Gent model predicts that with smooth quasi-shear waves propagate faster in sheared materials, and coalesce into shock when the prescribed transverse impact is greater than the initial shear state. The impact release or loading of shear may form quasi-pressure shocks owing to the coupling between the displacements, depending on initial deformation. The Gent model further predicts that the velocity of smooth quasi-pressure waves is a non-monotonic function of the axial strain, and their coalescence into shock intricately depends on the initial deformation. Notably, compressive impact may not be sufficient to induce a quasi-pressure shock—yet it may induce a quasi-shear shock, where tensile impact can trigger quasi-pressure shock—and may simultaneously trigger a quasi-shear shock. In agreement with Knowles (2002), who tackled the tensional problem with a kinetic approach, we find that the tensile impact must be greater than threshold value to induce shock. We characterize the dependency of this value on the initial deformation, and specifically find that the threshold is lower in the presence of pre-shear. These observations imply that the Gent model is suitable for the modeling of shocks in soft materials.

The interesting and more intricate aspects of finite amplitude wave reflection and transition from free boundaries and material interfaces are left for future studies (Nair and Nemat-Nasser, 1971; Agrawal and Bhattacharya, 2014).

Acknowledgments

We acknowledge the supports of the Israel Science Foundation, funded by the Israel Academy of Sciences and Humanities (Grant no. 1912/15), and the United States-Israel Binational Science Foundation (Grant no. 2014358).

Appendix A

We graphically illustrate how we obtain the values of M_U and Q_U for two of the examples in the body of the paper. Our first example is for the conditions $(M_I, Q_I, M_B, Q_B) = (0, 0, 0, 2.2)$. Note that since the material is unstrained, M and Q are uncoupled for the quasi-pressure wave. Hence, we know that the set of equations for smooth-smooth is not compatible, and therefore proceeded to solve the equations for shock-smooth waves. To this end, we solve Eq. (17)$_1$ and plot its solution in Fig. 9 (dashed brown curves). The value of $M_U(Q_U = Q_I = 0)$ is denoted by the diamond mark.

Our second example is for $(M_I, Q_I, M_B, Q_B) = (-0.6, 2, 0, 1)$. To solve the equations of smooth-smooth waves, we plot in Fig. 9 the numerical solutions to Eqs. (13) and (14) for (M, Q), obtained from Wolfram Mathematica 11.3 (2018). We determine the values of (M_U, Q_U) from the intersection between the curves. The circle, triangle and square correspond to Q_B, Q_U and Q_I, respectively. Furthermore, the values Q_B and Q_U are indicated in Fig. 4(a) by the circle and triangle marks, respectively, showing that condition (15) is satisfied for the quasi-shear wave. Similarly, the values of M_U and M_I are indicated in Fig. 5(a) by the as triangle and square marks, respectively, showing that condition (15) is satisfied for the quasi-pressure wave.

References

Aboudi, J., Benveniste, Y., 1973. One-dimensional finite amplitude wave propagation in a compressible elastic half-space. Int. J. Solids Struct. 9 (3), 363–378. https://doi.org/10.1016/0020-7683(73)90086-3. ISSN 0020–7683. http://www.sciencedirect.com/science/article/pii/0020768373900863.

Agrawal, V., Bhattacharya, K., 2014. Shock wave propagation through a model one dimensional heterogeneous medium. Int. J. Solids Struct. 51 (21), 3604–3618. https://doi.org/10.1016/j.ijsolstr.2014.06.021. ISSN 0020–7683. http://www.sciencedirect.

com/science/article/pii/S0020768314002534.
Bandyopadhyay, A., Vahabzadeh, S., Shivaram, A., Bose, S., 2015. Three-dimensional printing of biomaterials and soft materials. MRS Bull. 40 (12), 1162–1169. https://doi.org/10.1557/mrs.2015.274. ISSN 0883–7694.
Boulanger, P.H., Hayes, M., 1992. Finite-amplitude waves in deformed mooney-rivlin materials. Q. J. Mech. Appl. Math. 45 (4), 575–593. https://doi.org/10.1093/qjmam/45.4.575.
Carroll, M.M., 1967. Some results on finite amplitude elastic waves. Acta Mech. 3 (2), 167–181.
Carroll, M.M., 1974. Oscillatory shearing of nonlinearly elastic solids. Z. Angew. Math. Phys. ZAMP 25 (1), 83–88. https://doi.org/10.1007/BF01602111. ISSN 1420–9039.
Carroll, M.M., 1978. Finite amplitude standing waves in compressible elastic solids. J. Elast. 8 (3), 323–328. https://doi.org/10.1007/BF00130471. ISSN 1573–2681.
Catheline, S., Gennisson, J.L., Tanter, M., Fink, M., 2003. Observation of shock transverse waves in elastic media. Phys. Rev. Lett. 91, 164301. https://doi.org/10.1103/PhysRevLett.91.164301.
Cioroianu, A.R., Cornelis, S., 2013. Normal stresses in elastic networks. Phys. Rev. E 88, 052601. https://link.aps.org/doi/10.1103/PhysRevE.88.052601.
Davison, L., 1966. Propagation of plane waves of finite amplitude in elastic solids. J. Mech. Phys. Solids 14 (5), 249–270. https://doi.org/10.1016/0022-5096(66)90022-6. ISSN 0022–5096. http://www.sciencedirect.com/science/article/pii/0022509666900226.
Davison, L., 2008. Fundamentals of Shock Wave Propagation in Solids. Springer-Verlag, Berlin Heidelberg.
Deng, B., Raney, J.R., Tournat, V., Bertoldi, K., 2017. Elastic vector solitons in soft architected materials. Phys. Rev. Lett. 118, 204102.
Destrade, M., Saccomandi, G., 2005. Finite amplitude elastic waves propagating in compressible solids. Phys. Rev. E 72 (1), 16620.
Gent., A.N., 1996. A new constitutive relation for rubber. Rubber Chem. Technol. 69, 59–61.
Giammarinaro, B., Espíndola, D., Coulouvrat, F., Pinton, G., 2018. Focusing of shear shock waves. Phys. Rev. Appl. 9, 014011. https://doi.org/10.1103/PhysRevApplied.9.014011.
He, H., Cao, X., Dong, H., Ma, T., Payne, G.F., 2017. Reversible programing of soft matter with reconfigurable mechanical properties. Adv. Funct. Mater. 27 (13), 1605665. https://onlinelibrary.wiley.com/doi/abs/10.1002/adfm.201605665.
Horgan, C.O., 2015. The remarkable gent constitutive model for hyperelastic materials. Int. J. Non Linear Mech. 68, 9–16. https://doi.org/10.1016/j.ijnonlinmec.2014.05.010. ISSN 0020–7462. http://www.sciencedirect.com/science/article/pii/S0020746214001127.
Horgan, C.O., Murphy, J.G., 2017. Poynting and reverse poynting effects in soft materials. Soft Matter 13, 4916–4923. https://doi.org/10.1039/C7SM00992E.
Jacob, X., Catheline, S., Gennisson, J.-L., Barrière, C., Royer, D., Fink, M., 2007. Nonlinear shear wave interaction in soft solids. J. Acoust. Soc. Am. 122 (4), 1917–1926. https://doi.org/10.1121/1.2775871.
Kim, J., Kim, C., Song, Y., Jeong, S.-G., Kim, T.-S., Lee, C.-S., 2017. Reversible self-bending soft hydrogel microstructures with mechanically optimized designs. Chem. Eng. J. 321, 384–393. https://doi.org/10.1016/j.cej.2017.03.125. ISSN 1385–8947. http://www.sciencedirect.com/science/article/pii/S1385894717304928.
Knowles, J.K., 2002. Impact-induced tensile waves in a rubberlike material. SIAM J. Appl. Math. 62 (4), 1153–1175.
Kolsky, H., 1969. Production of tensile shock waves in stretched natural rubber. Nature 224 (5226), 1301.
Lints, M., Santos, S.D., Salupere, A., 2017. Solitary waves for non-destructive testing applications: delayed nonlinear time reversal signal processing optimization. Wave Motion 71, 101–112. https://doi.org/10.1016/j.wavemoti.2016.07.001. ISSN 0165–2125. http://www.sciencedirect.com/science/article/pii/S0165212516300701. Mathematical Modeling and Physical Dynamics of Solitary Waves: From Continuum Mechanics to Field Theory.
Lopez-Pamies, O., Castañeda, P.P., 2007. Homogenization-based constitutive models for porous elastomers and implications for macroscopic instabilities: ii—results. J. Mech. Phys. Solids 55 (8), 1702–1728. https://doi.org/10.1016/j.jmps.2007.01.008. ISSN 0022–5096. http://www.sciencedirect.com/science/article/pii/S0022509607000269.
Lustig, B., Shmuel, G., 2018. On the band gap universality of multiphase laminates and its applications. J. Mech. Phys. Solids 117, 37–53. https://doi.org/10.1016/j.jmps.2018.04.008. ISSN 0022–5096. http://www.sciencedirect.com/science/article/pii/S0022509618302321.
Nadkarni, N., Daraio, C., Kochmann, D.M., 2014. Dynamics of periodic mechanical structures containing bistable elastic elements: from elastic to solitary wave propagation. Phys. Rev. E 90 (2), 23204. https://doi.org/10.1103/PhysRevE.90.023204. http://link.aps.org/doi/10.1103/PhysRevE.90.023204.
Nair, S., Nemat-Nasser, S., 1971. On finite amplitude waves in heterogeneous elastic solids. Int. J. Eng. Sci. 9 (11), 1087–1105.
Niemczura, J., Ravi-Chandar, K., 2011a. On the response of rubbers at high strain rates—i. Simple waves. J. Mech. Phys. Solids 59 (2), 423–441. https://doi.org/10.1016/j.jmps.2007.01.008. ISSN 0022–5096. http://www.sciencedirect.com/science/article/pii/S0022509610001821.
Niemczura, J., Ravi-Chandar, K., 2011b. On the response of rubbers at high strain rates—II. Shock waves. J. Mech. Phys. Solids 59 (2), 442–456. https://doi.org/10.1016/j.jmps.2010.09.007. ISSN 0022–5096. http://www.sciencedirect.com/science/article/pii/S0022509610001833.
Puglisi, G., Saccomandi, G., 2015. The gent model for rubber-like materials: an appraisal for an ingenious and simple idea. Int. J. Non Linear Mech. 68, 17–24. https://doi.org/10.1016/j.ijnonlinmec.2014.05.007. ISSN 0020–7462. http://www.sciencedirect.com/science/article/pii/S0020746214001097.
Rajagopal, K.R., 1998. On a class of elastodynamic motions in a neo-Hookean elastic solid. Int. J. Non Linear Mech. 33 (3), 397–405. https://doi.org/10.1016/S0020-7462(97)00032-2. ISSN 0020–7462. http://www.sciencedirect.com/science/article/pii/S0020746297000322.
Raney, J., Nadkarni, N., Daraio, C., Kochmann, D.M., Lewis, J.A., Bertoldi, K., 2016. Stable propagation of mechanical signals in soft media using stored elastic energy. Proc. Natl. Acad. Sci. USA.
Scheidler, M., 2000. Universal relations for pressure-shear waves in nonlinear elastic solids. AIP Conf. Proc. 505 (1), 181–184. https://doi.org/10.1063/1.1303451. https://aip.scitation.org/doi/abs/10.1063/1.1303451.
Shmuel, G., Band, R., 2016. Universality of the frequency spectrum of laminates. J. Mech. Phys. Solids 92, 127–136. https://doi.org/10.1016/j.jmps.2016.04.001. ISSN 0022–5096.
Truby, R.L., Lewis, J.A., 2016. Printing soft matter in three dimensions. Nature 540, 371–378.
Wolfram, 2018. Research, inc. mathematica, version 11.3. champaign, IL.
Xin, F., Lu, T., 2016. Tensional acoustomechanical soft metamaterials. Sci. Rep. 6 (27432). EP –, 06 https://doi.org/10.1038/srep27432.
Yongchi, L., Ting, T.C.T., 1983. Plane waves in simple elastic solids and discontinuous dependence of solution on boundary conditions. Int. J. Solids Struct. 19 (11), 989–1008. https://doi.org/10.1016/0020-7683(83)90024-0. ISSN 0020–7683. http://www.sciencedirect.com/science/article/pii/0020768383900240.